

Hamiltonian, which generates  $U_p$  and satisfies  $\|U - U_p\| \leq d(I, U)2^n$ , as guaranteed by lemma 1, and where we have chosen  $p = 4^n$  as the penalty. Now divide the time interval  $[0, d(I, U)]$  up into a large number  $N$  of time intervals each of length  $\Delta = d(I, U)/N$ . Let  $U_p^j$  be the unitary operation generated by  $H_p(t)$  over the  $j$ th time interval, where  $j$  is an integer. Let  $U_M^j$  be the unitary operation generated by the corresponding mean Hamiltonian. Then lemma 2 implies that:

$$\|U_p^j - U_M^j\| \leq 2[e^{3\sqrt{2}n\Delta} - (1 + \frac{3}{\sqrt{2}}n\Delta)] \quad (9)$$

Lemma 3 implies that we can synthesize a unitary operation  $U_A^j$  using at most  $c_1 n^2/\Delta$  one- and two-qubit gates and satisfying  $\|U_M^j - U_A^j\| \leq c_2 n^4 \Delta^3$ .

Putting all these results together and applying the triangle inequality repeatedly, we obtain

$$\|U - U_A\| \leq \|U - U_p\| + \|U_p - U_A\| \quad (10)$$

$$\leq \frac{d(I, U)}{2^n} + \sum_{j=1}^N \|U_p^j - U_A^j\| \quad (11)$$

$$\leq \frac{d(I, U)}{2^n} + \sum_{j=1}^N (\|U_p^j - U_M^j\| + \|U_M^j - U_A^j\|) \quad (12)$$

$$\leq \frac{d(I, U)}{2^n} + 2 \frac{d(I, U)}{\Delta} \times \left[ e^{(3/\sqrt{2})n\Delta} - \left(1 + \frac{3}{\sqrt{2}}n\Delta\right) \right] + c_2 d(I, U) n^4 \Delta^2 \quad (13)$$

Provided we choose  $\Delta$  to scale at most as  $1/[n^2 d(I, U)]$ , we can ensure that the error in our approximation  $U_A$  to  $U$  is small, and the number of gates scales as  $n^6 d(I, U)^3$ .

Summing up, we have the following theorem (17): Using  $O(n^6 d(I, U)^3)$  one- and two-qubit gates, it is possible to synthesize a unitary  $U_A$  satisfying  $\|U - U_A\| \leq c$ , where  $c$  is any constant (e.g.,  $c = 1/10$ ).

Our results demonstrate that, up to polynomial factors, the optimal way of generating a unitary operation is to move along the minimal geodesic curve connecting  $I$  and  $U$ . Because the length of such geodesics also provides a lower bound on the minimal number of quantum gates required to generate  $U$ , as shown in (2), the geometric formulation offers an alternate approach, which may suggest efficient quantum algorithms or provide a way of proving that a given algorithm is indeed optimal.

It would, of course, be desirable to completely classify the geodesics of the metric we constructed. An infinite class of such geodesics has been constructed in (2) and is shown to have an intriguing connection to the problem of finding the closest vector in a lattice. A more complete classification of the geodesics could provide major insight on the potential power of quantum computation.

#### References and Notes

1. P. W. Shor, *Proceedings of the 35th Annual Symposium on Fundamentals of Computer Science* (IEEE Press, Los Alamitos, CA, 1994).
2. M. A. Nielsen, *Quant. Inf. Comput.*, in press (preprint available at <http://arxiv.org/abs/quant-ph/0502070>).
3. V. Jurdjevic, *Geometric Control Theory* (Cambridge Univ. Press, Cambridge, 1996).
4. N. Khaneja, R. Brockett, S. J. Glaser, *Phys. Rev. A* **63**, 032308 (2001).
5. N. Khaneja, S. J. Glaser, *Chem. Phys.* **267**, 11 (2001).
6. N. Khaneja, S. J. Glaser, R. Brockett, *Phys. Rev. A* **65**, 032301 (2002).
7. An alternate way of viewing this cost function is as a penalty metric of the kind used in sub-Riemannian geometry (18, p. 18).

8. The cost function has the property that  $F(\alpha H) = |\alpha|F(H)$ , where  $\alpha$  is any real number. This property and the chain rule imply invariance of the length with respect to reparameterization.
9. V. I. Arnold, B. A. Khesin, *Topological Methods in Hydrodynamics*, vol. 125 of *Applied Mathematical Sciences* (Springer, New York, 1998).
10. Our metric is superficially similar to the usual metric of Euclidean space, and it is tempting to suppose that geodesics must be straight lines, i.e., constant Hamiltonians. However, the Pauli coefficients for the Hamiltonian actually correspond to a changing local basis for the tangent space, not a fixed basis, and hence constant Hamiltonians do not, in general, give rise to geodesics.
11. J. Milnor, *Morse Theory* (Princeton Univ. Press, Princeton, NJ, 1969).
12. M. Berger, *A Panoramic View of Riemannian Geometry* (Springer, Berlin, 2003).
13. Proofs are available as supporting material on Science Online.
14. The operator norm of  $X$  is defined as  $\|X\| = \max_{|\psi\rangle} \langle \psi | X | \psi \rangle$ , where the maximization is over all normalized vectors,  $\langle \psi | \psi \rangle = 1$ .
15. The first inequality comes from the fact that there are  $9n(n-1)/2 + 3n$  one- and two-qubit terms.
16. M. A. Nielsen, I. L. Chuang, *Quantum Computation and Quantum Information* (Cambridge Univ. Press, Cambridge, 2000).
17. The overhead factors in this theorem may be substantially improved, e.g., by making use of higher order analyses in lemmas 1 to 3. However, the key point—that  $U$  can be accurately approximated with a number of gates that scales polynomially with  $d(I, U)$ —remains the same.
18. R. Montgomery, *A Tour of Subriemannian Geometries, Their Geodesics and Applications*, vol. 91 of *Mathematical Surveys and Monographs* (American Mathematical Society, Providence, RI, 2002).
19. We thank S. Aaronson, M. de Burgh, J. Dodd, C. Hill, A. Hines, A. Lund, L. Noakes, M. Sarovar, and B. Toner for helpful discussions and the Australian Research Council for funding. We are especially grateful to L. Noakes for pointing out to us the simplified form of the geodesic equation for right-invariant metrics.

#### Supporting Online Material

[www.sciencemag.org/cgi/content/full/311/5764/1133/DC1](http://www.sciencemag.org/cgi/content/full/311/5764/1133/DC1)  
SOM Text

19 October 2005; accepted 20 December 2005  
10.1126/science.1121541

## Effects of Solar Flares on the Ionosphere of Mars

Michael Mendillo,<sup>1</sup> Paul Withers,<sup>1\*</sup> David Hinson,<sup>2</sup> Henry Rishbeth,<sup>1,3</sup> Bodo Reinisch<sup>4</sup>

All planetary atmospheres respond to the enhanced x-rays and ultraviolet (UV) light emitted from the Sun during a flare. Yet only on Earth are observations so continuous that the consequences of these essentially unpredictable events can be measured reliably. Here, we report observations of solar flares, causing up to 200% enhancements to the ionosphere of Mars, as recorded by the Mars Global Surveyor in April 2001. Modeling the altitude dependence of these effects requires that relative enhancements in the soft x-ray fluxes far exceed those in the UV.

Sudden changes in the Sun's photon radiation and in the particles and fields of its solar wind reach Earth in about 8 min and a few days, respectively. These enhanced sources of energy cause sudden atmospheric disturbances and the auroral displays associated with longer lived geomagnetic storms. The recent

availability of spacecraft orbiting other planets has enabled studies of such effects on other worlds. A mass ejection from the Sun's corona in early November 2000 caused auroras on Earth, Jupiter, and Saturn during its month-long traverse through the solar system, providing a specific challenge to models that track solar wind density and magnetic

field enhancements (1). Increased x-ray emissions were observed from Jupiter and Saturn in November 2003 and January 2004, respectively, shortly after solar flares, thereby demonstrating the Sun's control of nonauroral x-ray emission from giant planets (2, 3). However, the direct response of another planetary atmosphere to solar flare photons, e.g., suddenly enhancing its ionosphere, has not been seen. Here, we report such an effect in the ionosphere of Mars.

Ions and electrons in a planet's ionosphere are produced by the photoionization of neutral

<sup>1</sup>Center for Space Physics, Boston University, Boston, MA 02215, USA. <sup>2</sup>Department of Electrical Engineering, Stanford University, Stanford, CA 94305, USA. <sup>3</sup>School of Physics and Astronomy, University of Southampton, Southampton SO17 1B, UK. <sup>4</sup>Center for Atmospheric Research, University of Massachusetts Lowell, Lowell, MA 01854, USA.

\*To whom correspondence should be addressed. E-mail: [withers@bu.edu](mailto:withers@bu.edu)

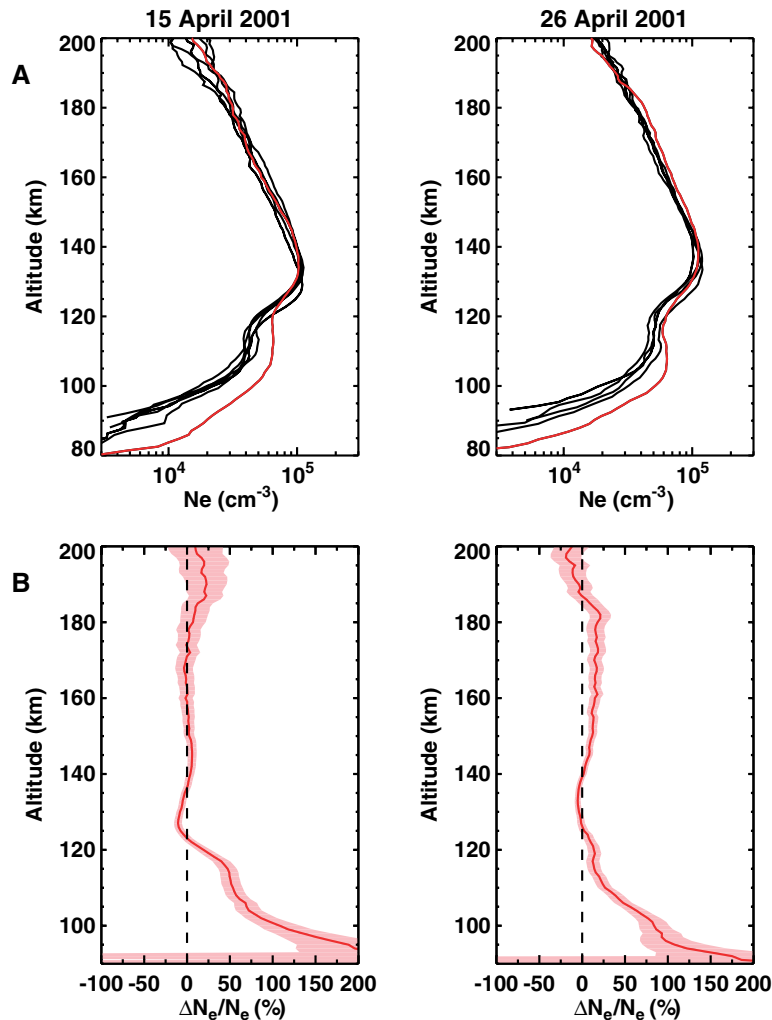
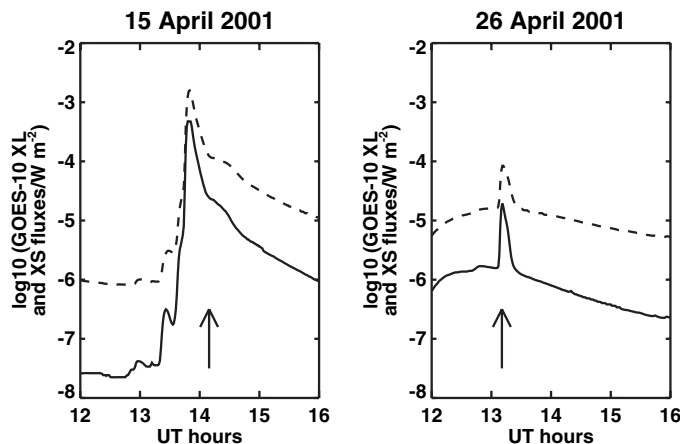


**Fig. 1.** (A) Electron density profiles on Mars obtained for 15 April and 26 April 2001. Measurement uncertainty is several thousand electrons/cm<sup>3</sup>, and thus the two profiles in red [14:15 and 13:16 universal time (UT), respectively] show statistically significant departures at low altitudes because of solar flares. On 15 April, there were five MGS profiles before the flare, at 02:28, 06:23, 08:21, 10:19, and 12:17 UT, and none after the flare; on 26 April, preflare profiles were available at 09:20 and 11:18 UT, and postflare, at 17:11 and 19:09 UT. (B) Percentage differences between the flare-affected profiles and the averages of the other profiles on each day. The shadings give the 1-σ standard error in the relative change in N<sub>e</sub>.

**Fig. 2.** Solar x-ray fluxes on 15 and 26 April 2001 measured by the GOES spacecraft at Earth for two wavelength bands (11): XS (0.5 to 3 Å), solid line, and XL (1 to 8 Å), dashed line. The peak fluxes at Earth occurred at 13:50 UT and 13:10 UT, respectively. The solar fluxes incident upon Mars at the times of the flare-affected profiles in Fig. 1 are marked by arrows.



species by solar extreme ultraviolet (EUV) and x-ray photons (4, 5). The ionizing solar flux and thus the ionosphere are variable on many time scales. The most important is the 11-year solar cycle, whereas the shortest is the solar flare, an impulsive emission of photons that peaks within minutes and takes tens of minutes, and perhaps hours, to decay to preflare levels. Flares affect Earth's atmosphere and radio propagation controlled by its ionosphere. Such effects have been used historically as proxies to deduce how the Sun's EUV and x-rays changed during a flare (6, 7).

Artificial satellites passing by or orbiting Mars are required to conduct radio soundings of its ionosphere. The 443 published measurements obtained by U.S. and Soviet probes between 1965 and 1980 led to a basic understanding of the structure of its electron density profile (5, 8, 9). Depending on solar zenith angle, the martian ionosphere has a main peak between 120 and 140 km produced by ultraviolet photons in the wavelength range from 200 to 800 Å. A lower peak, or ledge, at 90 to 110 km is produced by x-rays (<100 Å). In 1998, the Mars Global Surveyor (MGS), with its radio science experiment (10), was inserted into orbit around Mars. By 2001, MGS made 1867 measurements of the martian ionosphere, enabling investigation of ionospheric variability and its causes (9). MGS transmits a 3.6-cm-wavelength radio signal to Earth, and, as it passes behind or emerges from the far side of the planet, the propagation is perturbed by the neutral atmosphere and the ionosphere of Mars. The observable effect is a Doppler shift in the frequency of the signal received on Earth, and vertical profiles of electron density can be retrieved from such data.

Six MGS profiles of electron density versus height, N<sub>e</sub>(h), were measured on 15 April 2001, and five were measured on 26 April 2001 (Fig. 1). All the profiles refer essentially to the same latitude (84°N) and local time (08:40 LT) on Mars but were made at different longitudes at ~2-hour intervals. All profiles show a stable pair of layers: the main one near 130 km and a secondary peak between 105 and 110 km. Day-to-day variability is 5 to 7% at the main peak and ~10% at the lower peak (8). In one case on each day, the electron densities at and below the secondary peak are enhanced by 50 to 200%. We have traced these dramatic changes to x-rays from solar flares that occurred within minutes of each observation (Fig. 2).

The Geostationary Operational Environmental Satellites (GOES) (11) in orbit about Earth make continuous observations of solar x-rays. The X14.4 flare of 15 April was the second strongest in 2001, whereas the M7.8 flare of 26 April was far more moderate. The Sun-Earth-Mars angle was only ~26° at these times, and so it is reasonable to apply the solar irradiance (photon flux versus wavelength) measured at Earth to Mars with a 4.5-min

delay. Thus, the peak fluxes on 15 and 26 April reached Mars  $\sim 20$  min and  $\sim 90$  s, respectively, before the profiles highlighted (Fig. 1).

Although GOES x-rays can be enhanced by orders of magnitude during a flare, they are too energetic (“hard”) to produce the ionospheric enhancements shown. They penetrate to altitudes around 60 km, where unambiguous MGS measurements of electron density are not available. Very large relative increases in  $N_e$  must have occurred suddenly at these low heights. At the altitudes of the enhancements observed by MGS, ionization is caused by softer x-rays in the 18- to 50-Å range (9, 12), a wavelength region not measured by GOES. At about 110 km, production by photons ( $P = F_s \sigma \eta N$ ) equals chemical loss ( $L = \alpha N_e^2$ ), where

$F_s$  is the effective flux of solar photons that cause ionization,  $\sigma$  is the cross section for ionization of  $\text{CO}_2$ ,  $\eta$  is the number of ion-electron pairs created per x-ray photon absorbed,  $N$  is the concentration of  $\text{CO}_2$ ,  $\alpha$  is the dissociative recombination coefficient for  $\text{O}_2^+$  and electrons, and  $N_e$  is the electron density. Thus, for an observed flare-induced electron density ( $N_e^f$ ) 1.5 times the preflare value ( $N_e^o$ ) at 110 km, the solar flare’s ionizing flux ( $F_s^f$ ) with respect to its value before the flare ( $F_s^o$ ) would be

$$F_s^f / F_s^o = (N_e^f / N_e^o)^2 = (1.5)^2 = 2.25 \quad (1)$$

Increases by factors of 2 to 3 in the Sun’s soft x-ray flux during a flare are well within observed variabilities (13).

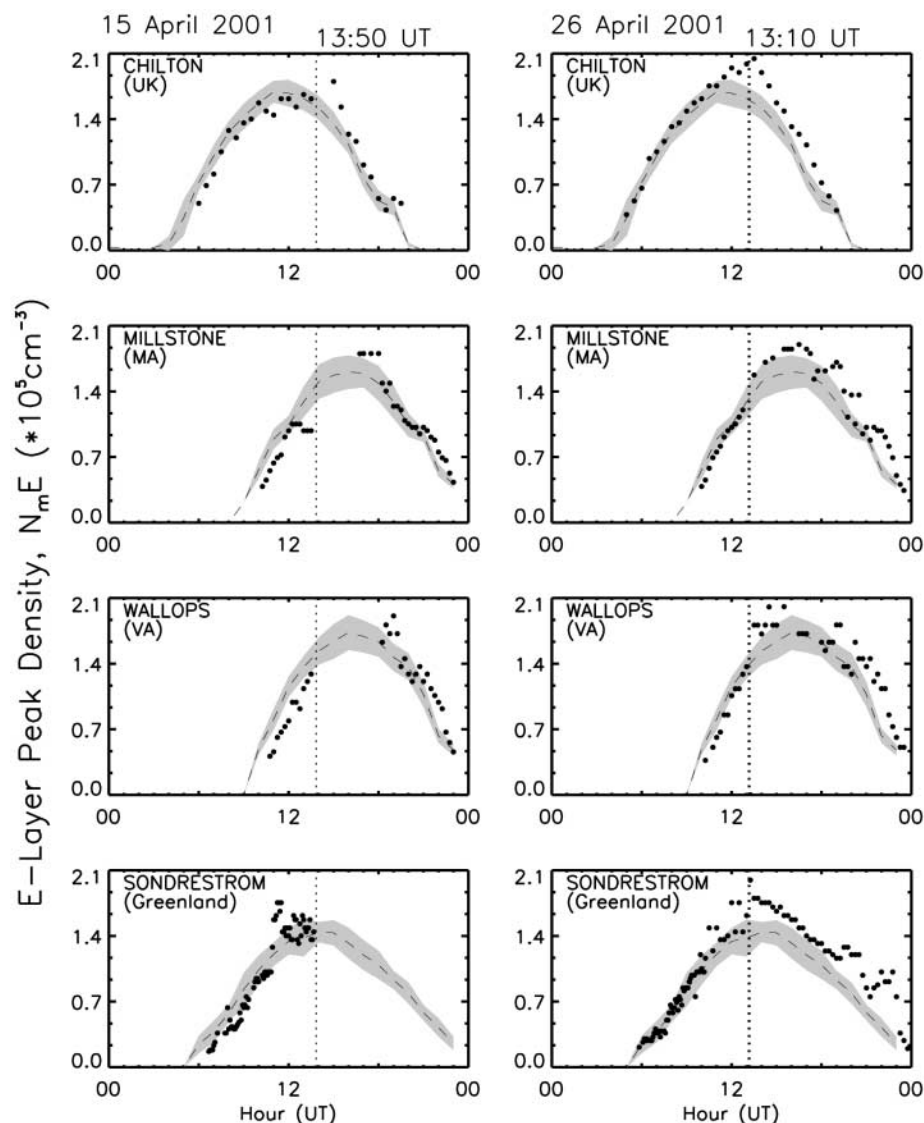


**Fig. 3.** The maximum electron densities of the Earth’s E layer ( $N_m E$ ) for 15 April and 26 April 2001. For each station, the monthly mean pattern is given by the dashed lines, their standard deviations ( $1 \sigma$ ) by the shading, and individual data points by dots (scaled to 0.1 MHz, giving  $\sim 10\%$  uncertainty). The vertical dotted lines show the times of peak flare fluxes. At the highest latitude ionosonde station (Sondrestrom, Greenland), there is additional preflare E layer variability caused by auroral activity and sporadic E layers.

The Solar and Heliospheric Observatory (SOHO) spacecraft also observes the Sun from Earth orbit, but it only had data for 15 April. Those data show that at the time of the MGS measurements EUV fluxes (260 to 340 Å) were enhanced by only  $\sim 10\%$ , whereas fluxes integrated over the broad wavelength range from 1 to 500 Å (soft x-rays plus EUV) increased by  $\sim 50\%$ . This trend suggests greater enhancements in the 1- to 50-Å range (soft x-rays only) (14), consistent with the observed changes in the martian ionosphere being confined to lower heights.

The responses of the martian ionosphere were similar for these two flares despite their very different peak fluxes. This is because the postflare  $N_e(h)$  profile for the weaker event (26 April) was measured just 90 s after the peak x-ray flux, whereas for the far stronger event on 15 April the MGS observation was made 20 min into the flare’s decay phase. The GOES fluxes of hard x-rays were of comparable magnitude at these times, and thus it is reasonable that the soft x-rays fluxes were also similar.

To show that such flares have consequences on Earth, we searched for terrestrial measurements made at ionosonde sites that were in daylight at the times of both flares. An ionosonde (15) is essentially a radar for electrons that transmits frequencies in the 1- to 30-MHz range and records the time delays of echoes reflected by the ionosphere. Earth’s ionosphere has multiple layers, with a main high-altitude peak near 300 km (called the F layer) produced primarily by EUV, an E layer near 100 km produced by soft x-rays and EUV, and a D layer near 70 km produced by hard x-rays. For comparison with Mars’s secondary peak, the terrestrial E layer is the most appropriate one because of the wavelengths that produce it and because the F layer is heavily influenced by transport processes. We plotted the E layer maximum electron density ( $N_m E$ ) versus LT in Fig. 3. The four data sets span high latitudes (Sondrestrom, Greenland) to midlatitudes (Chilton, UK; Millstone Hill, MA; and Wallops Island, VA). The solar zenith angle at Sondrestrom for these flares was about  $61^\circ$ , somewhat comparable to the  $72^\circ$  at the MGS high-latitude observing location on Mars.

The flare of 15 April was so severe that these instruments were unable to observe the ionospheric layers. Enhanced electron densities in the D layer produced by the hard x-rays caused absorption of the radio waves transmitted, thus preventing soundings of the overlying E and F layers. If an ionosonde had been operating on Mars, similar effects would have occurred there as well. This D layer absorption was so severe on Earth that observations were not possible for the rest of the day at Sondrestrom, for 3 hours at Millstone Hill and Wallops Island, and for only an hour at Chilton. When observations resumed at the latter sites,  $N_m E$  was higher than might be expected had the flare not occurred. Thus,

the major signature of the 15 April flare on Earth was the elimination of reliable ionospheric data.

More continuous data sets exist for the 26 April flare, and they show the expected enhancements of the E layer electron densities by the flare. At Sondrestrom, the site most appropriate for comparisons with MGS at Mars, the electron density increased by ~45%. Because the E layer is caused by both EUV and soft x-rays and the EUV changed only slightly, the Sondrestrom results must be due to the more-than-double effective ionizing fluxes, in agreement with Eq. 1 applied at Mars. We conclude that these two flares produced near-simultaneous enhancements in the ionospheres of Earth and Mars and that the greater relative increase at lower altitudes in Mars'  $N_e(h)$  is consistent with the typical flare spectrum of greater relative flux increases at shorter wavelengths. The  $N_e$  increase at Mars is also consistent with the enhancement at its corresponding site on Earth.

The detection of solar flare effects in the martian ionosphere has important consequences. Previous observations and modeling of the responses of planetary ionospheres to changes in solar flux have generally compared solar maximum and minimum conditions. Varying solar fluxes also modify the neutral atmosphere, and thus ionospheric changes result from two highly coupled processes. Although simulations

can separate the dependence on each of these parameters, validation from observations over a solar cycle cannot. The observations presented here decouple changes in photon flux due to a flare from far slower changes in the neutral atmosphere, thereby providing a way to constrain photochemistry on two planets simultaneously. This is particularly important for x-ray photons that carry energy far above that needed to ionize an atom or molecule. In such cases, the electron liberated by ionization has so much extra energy that it ionizes other atoms and molecules via collisions. This secondary ionization by photoelectrons is an amplification effect that needs validation throughout the solar system. For Venus, Earth, and Mars, where ionospheric layers have identical end product ions ( $O_2^+$ ), solar flares offer tests for both primary and secondary ionization coupled to an identical chemical loss mechanism. Calculations using the same solar flare input thus provide constraints not possible at a single planet.

#### References and Notes

1. R. Prange *et al.*, *Nature* **432**, 78 (2004).
2. A. Bhardwaj *et al.*, *Geophys. Res. Lett.* **32**, 10.1029/2004GL021497 (2005).
3. A. Bhardwaj *et al.*, *Astrophys. J.* **624**, L121 (2005).
4. H. Rishbeth, O. K. Garriott, *Introduction to Ionospheric Physics* (Academic Press, New York, 1969).
5. R. Schunk, A. Nagy, *Ionospheres* (Cambridge Univ. Press, Cambridge, 2000).

6. R. F. Donnelly, *Sol. Phys.* **20**, 188 (1971).
7. N. R. Thomson, C. J. Rodger, R. L. Dowden, *Geophys. Res. Lett.* **31**, 10.1029/2003GL019345 (2004).
8. M. Mendillo, S. Smith, J. Wroten, H. Rishbeth, D. Hinson, *J. Geophys. Res.* **108**, 10.1029/2003JA009961 (2003).
9. C. R. Martinis, J. K. Wilson, M. Mendillo, *J. Geophys. Res.* **108**, 10.1029/2003JA009973 (2003).
10. D. P. Hinson, R. A. Simpson, J. D. Twicken, G. L. Tyler, F. M. Flasar, *J. Geophys. Res.* **104**, 26997 (1999).
11. P. L. Bornmann *et al.*, *Proc. SPIE* **2812**, 309 (1996).
12. J. Fox, *J. Geophys. Res.* **109**, 10.1029/2004JA010380 (2004).
13. P. C. Chamberlin, T. N. Woods, F. G. Eparvier, abstract SA34A.08, 2005 American Geophysical Union (AGU) Fall Meeting, San Francisco, CA, 5 to 9 December 2005.
14. D. L. Judge, H. S. Ogawa, D. R. McMullin, P. Gangopadhyay, J. M. Pap, *Adv. Space Res.* **29**, 1963 (2002).
15. B. W. Reinisch, in *Modern Ionospheric Science*, H. Kohl, R. Ruster, K. Schlegel, Eds. (European Geophysical Society, Katlenburg-Lindau, Germany, 1996), pp. 440–458.
16. At Boston University, this work was supported by NASA's Mars Data Analysis program (M.M., H.R., and P.W.) and from NSF's Coupling, Energetics, and Dynamics of Atmospheric Regions program (P.W.). At Stanford University, support is from the NASA MGS program. At the University of Massachusetts, Lowell, support for the ionosonde observations comes from U.S. Air Force grant no. f19628-C-0092. We are grateful for data analysis provided by J. Wroten (Boston University) and G. Khmyrov (University of Massachusetts, Lowell) and acknowledge use of GOES data from <http://sec.noaa.gov/Data/goes.html> and SOHO data from [www.usc.edu/dept/space\\_science/semdata.htm](http://www.usc.edu/dept/space_science/semdata.htm).

1 November 2005; accepted 13 January 2006  
10.1126/science.1122099

## Anthropogenic and Natural Influences in the Evolution of Lower Stratospheric Cooling

V. Ramaswamy,<sup>1</sup> M. D. Schwarzkopf,<sup>1</sup> W. J. Randel,<sup>2</sup> B. D. Santer,<sup>3</sup> B. J. Soden,<sup>4</sup> G. L. Stenchikov<sup>5</sup>

Observations reveal that the substantial cooling of the global lower stratosphere over 1979–2003 occurred in two pronounced steplike transitions. These arose in the aftermath of two major volcanic eruptions, with each cooling transition being followed by a period of relatively steady temperatures. Climate model simulations indicate that the space-time structure of the observed cooling is largely attributable to the combined effect of changes in both anthropogenic factors (ozone depletion and increases in well-mixed greenhouse gases) and natural factors (solar irradiance variation and volcanic aerosols). The anthropogenic factors drove the overall cooling during the period, and the natural ones modulated the evolution of the cooling.

The global lower stratosphere—the region of the atmosphere from ~12 to 22 km above the surface—has cooled substantially over the past two decades (1–5). The difference in temperature between 2000 and 1979 has been ascribed mainly to ozone depletion and increases in well-mixed greenhouse gases (4, 6–10). Observations indicate that the decrease in temperature was steplike rather than a steady decline (1, 3). Although the overall trend in temperature has been modeled previously (5, 9, 10), the steplike structure and

the evolution of the cooling pattern in the observed global temperature time series has not been explained in terms of specific physical causes, whether these be external forcing and/or internal variability of the climate system. Thus, attribution of the unusual cooling features observed during the 1980s and 1990s has yet to be addressed, along with potential implications for the future.

We used a coupled atmosphere-ocean model (11–13) to demonstrate that the complex space-time pattern of the lower stratospheric tem-

perature anomalies is a consequence of the combined temporal changes in natural forcings [solar irradiance (14) and volcanic aerosols (15)] and anthropogenic forcings [well-mixed greenhouse gases (16), stratospheric (17) and tropospheric ozone (18), tropospheric aerosols (18), and land use (13)].

We performed five separate experiments to investigate the contributions of different forcing mechanisms to changes in lower stratospheric temperature: (i) natural plus anthropogenic (AllForc), (ii) natural (Nat), (iii) well-mixed greenhouse gases (Wmgg), (iv) well-mixed greenhouse gases plus stratospheric and tropospheric ozone (WmggO3), and (v) anthropogenic (Anth; that is, WmggO3 plus tropospheric aerosols and land-use change). For each case, an ensemble of simulations was performed. Individual ensemble members started from different points of a long control simulation with a fixed preindustrial (1860) atmospheric composition and were then integrated from 1861 through 2003. There were five ensemble members for (i);

<sup>1</sup>National Oceanic and Atmospheric Administration/Geophysical Fluid Dynamics Laboratory, Princeton, NJ 08542, USA.

<sup>2</sup>National Center for Atmospheric Research, Boulder, CO 80303, USA. <sup>3</sup>Program for Climate Model Diagnosis and Intercomparison, Lawrence Livermore National Laboratory, Livermore, CA 94550, USA. <sup>4</sup>Rosentiel School for Marine and Atmospheric Science, University of Miami, Miami, FL 33149, USA. <sup>5</sup>Department of Environmental Sciences, Rutgers University, New Brunswick, NJ 08901, USA.